
SPECTROSCOPY
OF CONDENSED MATTER

Determination of Rate Constants and the Mechanism of Phototransformations of Metalloporphyrins by Solving the Inverse Photokinetic Problem

I. V. Stanishevsky^{a,*} and S. M. Arabei^a

^a Belarusian State Agrarian Technical University, Minsk, 220023 Belarus

*e-mail: ivanstanisheuski@mail.ru

Received June 23, 2020; revised August 28, 2020; accepted September 24, 2020

Abstract—Fluorescence kinetics of some substituted Zn- and Mg-porphyrins in solid polymeric films upon excitation by two-step-wise rectangular laser pulses and at 293 K are studied by methods of the inverse kinetic problem. The experimental nonmonotonic kinetic curves are approximated by simulated ones within the framework of a six-level energy scheme describing reversible interconversions of two complexes. The maximum correspondence between experimental and simulated curves is obtained by iterative optimization using the Nelder–Mead algorithm. Based on statistically estimated values of rate constants and parameters of the considered models, an interpretation of the observed kinetics is presented and a conclusion is drawn that the interconversions are caused by the process of reversible extraligation of the central metal ion; the process occurs in the excited triplet T_1 state.

Keywords: inverse kinetic problem, inverse photokinetic problem, two-step-wise rectangular photoexcitation pulses, estimation of photokinetic parameters, fluorescence fading, fluorescence antifading, extraligation, Nelder–Mead algorithm

DOI: 10.1134/S0030400X21020156

INTRODUCTION

Most of investigations of the afterglow kinetics, in particular, for organic luminescent compounds under pulse photoexcitation (PhE), are directed to acquisition of information about rates of the decay and formation of excited electron states, as well as rates of photophysical and photochemical processes. The performed nonlinear regression analysis of curves is in fact the initial and single stage of the consistent formal-kinetic approach defined as the inverse kinetic problem (IKP) [1–3]. The full algorithm of the IKP solution is more complicated and much more resource-intensive: at subsequent stages, estimation of kinetic parameters or/and discrimination of hypotheses are carried out [1]. In both cases, first, the mathematical (hypothetic) model of the photoprocess is specified in the form of a system of differential equations (SDE). Then, the problem of minimization (optimization) of the objective function (OF)—the function of mismatch between the experimental and model curve—is solved by numerical iterative methods. Thus, the IKP is formally the problem of finding values of kinetic and other calculated parameters that afford the best statistical description of experimental data at the physical sense of the hypothetical model. It is known that, for various reasons, the IKP is ill-posed one because it has no unique solution [1–4] since: the

OF can reach a minimum for many sets of model parameters. The long time of the OF optimization is often an additional difficulty due to the necessity of multiple integration of the SDE (in many cases, of the stiff type).

It should be noted that the number of physico-chemical investigations devoted to estimation of model parameters within the framework of the formal-kinetic approach is very insignificant [5–8]. In most works, the IKPs were solved by approximated methods. This state of the problem, which is preserved for quite many years, is explained by a series of circumstances: the absence of necessary experimental methods and ready-to-use software algorithms, as well as high requirements to the computational power of computers with an increase in the number of estimated parameters.

In [9–12], a new method for the determination of rate constants of photoinduced reactions in organic and complex compounds was proposed. The method is based on the formal-kinetic approach to solving inverse photokinetic problems (IPKPs). Those works became a continuation of model computer experiments demonstrating that using PhE with a two-step-wise rectangular profile allows one to considerably increase informativeness of the observed kinetics [13, 14]. The stages of solving the IPKP by numerical

methods in [9, 10] included (i) finding process characteristic rates for monotonic fragments (stages) of the kinetic curves [15, 16]; (ii) integration of linear systems of ordinary differential equations (LSODE) [17]; and (iii) minimization of the matching OF by the iterative Nelder–Mead gradientless (derivative-free) optimization algorithm [18, 19]. These stages made it possible to determine constants of extraligation (axial extracoordination) rates, ratio of initial concentrations of interrelated centers, and other parameters for some metalorganic luminophores.

In this work, it is reported about the analysis of composite nonmonotonic kinetic fluorescence curves of some metalloporphyrins in solid organic polymeric matrices under PhE. The analysis is carried out using two-step-wise rectangular pulses and based on the IPKP solution. The applied calculation methods made it possible to determine rate constants controlling interconversion processes of metal complexes of tetrapyrrole macrocycles, as well as to establish the phototransformation mechanism caused by the reversible process of axial extraligation of the central metal ion. The work also deals with some methodological issues related to the numerical solution of the IPKP.

EXPERIMENTAL

Objects of Study and Experimental Technique

The following porphyrin metal complexes were studied: Zn-tetra-(*tert*-butylbenzo)porphine (Zn-(*t*-Bu)₄-TBP), Zn-tetrabenzoporphine (Zn-TBP), Mg-tetrabenzoporphine (Mg-TBP), and Zn-octaethylporphine (Zn-OEP). The chemical structure of Zn-(*t*-Bu)₄-TBP is shown in the inset of Fig. 1, and the structures of other metal complexes were presented in [20]. The electron spectra of absorption and fluorescence of the studied compounds were presented in [21]. Porphyrin-dyed thin polyvinyl butyral (PVB) films were prepared according to the technique described in [22] and studied at room temperature. Metal porphyrins were excited in the Soret band region by a laser diode ($\lambda_{\text{gen}} = 405 \text{ nm}$) generating a sequence of pulses; the intensity of each of them in time had a two-step-wise rectangular profile. The pulse duration was specified from 10^{-2} s and longer; their repetition frequency, in the range from 1 to 0.01 Hz. The long-term temperature stability of the photopulse intensity profile was improved by circuitry methods of laser current thermocompensation. Radiation with a power of $\approx 1 \text{ mW}$ was focused on the sample to a spot with an area of $\approx 0.1 \text{ mm}^2$. The change in the fluorescence intensity of metal porphyrins in time (below in the text, fluorescence kinetics) was detected in the maximum of the 0–0 band of the $S_1 \rightarrow S_0$ transition. The typical width of the band was 350 cm^{-1} at the spectral slit width of the recording monochromator (MDR-23) $\approx 3.0 \text{ nm}$. Along with this, the time profile of the laser intensity was controlled by measuring the

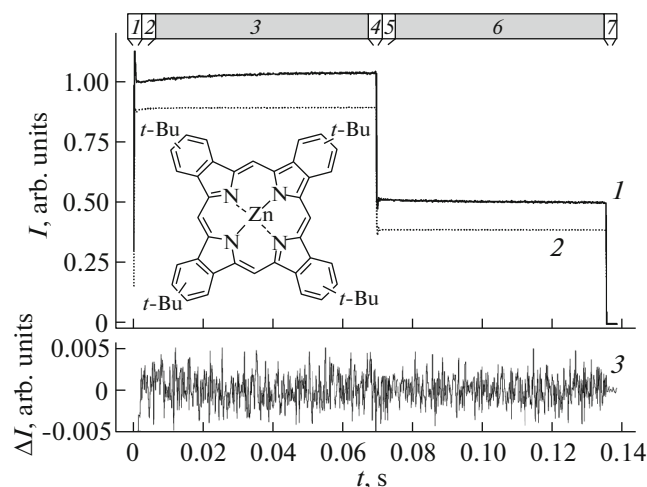


Fig. 1. (1) Fluorescence kinetics of Zn-(*t*-Bu)₄-TBP in a PVB film at $T = 293 \text{ K}$, $\lambda_{\text{det}} = 632 \text{ nm}$, and $\lambda_{\text{exc}} = 405 \text{ nm}$, (2) PhE intensity profile, and (3) relative difference between intensities of the experimental and optimized kinetic curves. The inset depicts the Zn-(*t*-Bu)₄-TBP structure.

luminescence kinetics of the Rhodamine B solution in ethanol at a concentration of less than 10^{-5} mol/L . Typically, the kinetic curves consisted of ≈ 800 samples of the photomultiplier tube (PMT) current with an interval $\Delta t = 10^{-5} - 10^{-3} \text{ s}$ between them. To reduce noises, the kinetic curves were accumulated and averaged typically over 25–100 laser pulses; the laser intensity profile, over 400–1000 pulses. The resulting typical noise amplitude was less than 0.005 of the maximum intensity of the kinetic curves. More details about the experimental technique were given in [10, 13, 14].

Numerical Calculations

The computational procedures of all IPKP stages were carried out in the Scilab environment, version 5.52 [23]. The characteristic rates of the processes were determined for monotonic stages of kinetic curves by the grid algorithms of nonlinear regression [15, 16]. Along with this, approximation curves in some calculations were used as smoothed initial curves. Integration of LSODE in the iterative optimization cycles was performed using the *LSODE Scilab*-procedure (the *stiff* method) [17]. To accelerate the integration, the LSODE Jacobian was specified in the explicit form and values of the *ODEOPTIONS* vector governing the computations and specifying their error were selected. The model kinetic fluorescence curve was represented as a functional in the form of superpositions of LSODE solutions. The OF was specified in the form of the Euclidean norm of mismatching between the vectors of the experimental and model kinetics,

$$\text{OF} = \sqrt{\sum_i (I_i^{\text{exper}} - I_i^{\text{calc}})^2},$$

and minimized by the derivative-free (deformed polyhedron) Nelder–Mead algorithm [18]. It was chosen due to the possibility of applying to nonmonotonic and noisy functions, as well as simple implementation and small number of iterations required for reaching the termination criterion as compared to other gradientless algorithms [19]. Instead of the *neldermead_new* program built in Scilab and implementing the Nelder–Mead algorithm, the *anms* procedure [24], more convenient for modification, was used. In view of the noticeable decrease in the algorithm efficiency with an increase in the dimension of the problem, the number of estimated parameters was maximally restricted. The reduction of their number was also favored by the fact that some parameters could be expressed as a fraction or combination of other parameters. Typically, their number did not exceed 10. In the start of optimization, the parameter vector was a result of elementwise product of the vector of their initial values and vector of ones factors varied by the algorithms as scale factors. After the optimization termination, the vector of initial values of the parameters was elementwise multiplied by the vector of optimized scale factors. This product served as the vector of initial parameters for the next optimization. For the vector describing the intensity profile of the PhE pulse, its own scale factor was optimized. Note that it is the use of the measured PhE profile for the calculation of the model fluorescence kinetics that made it possible to approximate the experimental kinetics by the model one.

The graphical algorithm of the IPKP solution by the Nelder–Mead iterative optimization method was presented in [12]. After the multiple sequential start of the optimization procedure or parallel execution of several procedures with different vectors of initial parameters, the obtained optimized parameter vectors were averaged. Calculation of the IPKP for one compound required not less than 20 starts of the optimization procedure or, totally, not less than 50000 iterations. The time of one iteration was determined mainly by the time of LSODE integration at thresholds of the absolute (*atol*) and relative (*rtol*) estimated errors of 10^{-8} and 10^{-6} , respectively, and lasted ~ 1 s on a computer with an Intel processor operated at of 3.5–4.2 GHz.

In addition to main calculations, the following auxiliary techniques and methods were used. The experimental curves and PhE profile were replaced by model ones, and optimization was carried out to obtain the maximum approximation of varied parameters to given ones. At the initial stage of the simulation, this made it possible to verify the monoexponentiality of all stages of nonmonotonic kinetics; at the stages of parameter estimation and choice of the physical model, this allowed one (i) to compare optimization results for different models; (ii) to reveal how the solution is sensitive to deviation of parameters; (iii) to estimate the effect of the noise on the solution; and (4) to

select parameters of the optimization algorithm with the aim to reduce the computational time.

Based on the summary of results of the IPKP solution, the following rather important information was obtained. Varying parameters of control for the simplex β (expansion), γ (contraction), and δ (shrink) allows one in some cases to reduce final OF values. The idea of centroid perturbation (the arithmetic mean of best vertices) in the form of its insignificant distortion in every iteration cycle [25] turned out to be fruitful; this allows the simplex to get out of local minima. The efficiency of the method considerably increases with a decrease in noisiness of kinetic curves. For example, when using smooth model curves, the final optimized values of parameters almost coincided with values taken for the synthesis of the curves.

For systems that are simpler than the model LSODE, exact analytical solutions were found using the *Maxima* computer algebra system [26]. They made it possible to reveal functional relationships, on the one hand, between process rates and, on the other hand, rate constants and concentrations of molecules of mutually transforming centers.

RESULTS AND DISCUSSION

For all samples, fluorescence kinetics with a specific profile differing from the PhE profile was observed. It repeated from pulse to pulse and depended on the PhE power. A typical kinetic curve, in particular, for Zn-(*t*-Bu)₄-TBP, as well as the PhE intensity profile, are presented in Fig. 1.

Determination of Characteristic Rates of Processes

On each curve, one could distinguish seven stages numbered from 1 to 7 (as an example, see Fig. 1). Stages 1, 4, and 7 corresponded to a rapid change in the intensity as a response to the stepwise change in the PhE.

Stages 2 and 5 were unambiguously characterized as photophysical fluorescence fading and antifading (FF and AF) of fluorescence, respectively; they were considered in detail in [13, 14]. The FF and AF are caused by processes of changes in the population of the T_1 state with simultaneous antipate change in the population of the ground state S_0 and, therefore, excited S_1 state. Stages 2 and 5 are seen more clearly for a shortened PhE pulse (Fig. 2). Results of the analysis of the kinetics in the form of magnitudes of the characteristic FF and AF rate distribution are presented in the inset of Fig. 2. The broadening of the bands is caused mainly by noisiness of the curves. Magnitude maximums of other compounds lay in the range of rates from 6×10^3 to 1×10^5 s⁻¹. From the presented kinetics, one can quite accurately estimate deactivation rate constants of the T_1 state (p) and PhE (k_{exc}). It is known [13] that the FF rate ($rate_{\text{FF}}$) is determined by the expression $rate_{\text{FF}} = p + k_{\text{exc}}Q$ in which Q is the quantum yield of the formation of T_1 ,

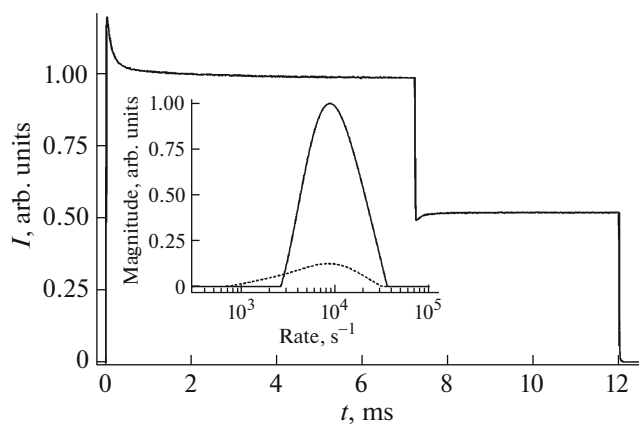


Fig. 2. Fluorescence kinetics of Zn-(*t*-Bu)₄-TBP in a PVB film at $T = 293$ K, $\lambda_{\text{det}} = 632$ nm, and $\lambda_{\text{exc}} = 405$ nm. The inset depicts results of the *CONTIN*-calculations: FF (the solid curve) and AF (the dashed curve).

and the relative amplitude of the FF peak (Δ_{FF}) is expressed by the ratio $\Delta_{\text{FF}} = p/k_{\text{exc}}Q$.

Stages 3 and 6 demonstrated a relatively slow increase and decrease in the fluorescence, respectively, and pointed to the occurrence of slow photoprocesses of other nature along with rapid photophysical processes of stages 2 and 5 in the system. Typical rates of stage 3 amounted to ~ 35 – 50 s⁻¹; rates of stage 6, to ~ 13 – 25 s⁻¹. The considerable resemblance of the fluorescence kinetics at these stages and luminescence kinetics of the Eu³⁺ complex [10] made it possible to suppose that the ensemble of fluorophores is chemically inhomogeneous and some of its subensembles convert into each other. An additional argument for this hypothesis is indicated by the kinetics of NH-phototautomerism of free base porphyrins at low temperatures [27]. In addition, the numerical and exact analytical solution for the population of the S_1 level (fluorescence intensity) at stepwise PhE in the three-level model approximation, i.e., for a homogeneous ensemble, has the form of a descending monotonic curve [9, 28]. Additional levels in such a model change only the monotonicity character.

Estimation of Model Parameters and Rate Constants

To determine the causes of kinetics nonmonotonicity, i.e., the appearance of stages 3 and 6, the formal-kinetic approach was used. Several hypothetical models of photoprocesses were considered; for reasons of minimalism, they consisted of two types of chemically nonequivalent complexes (K1 and K2). The models differed in ways of PhE energy deactivation. The scheme of energy levels and ways of deactivation of PhE energy for one of them is presented in Fig. 3. It describes the K1 \leftrightarrow K2 conversions with the participation of the $T_1^{(1)} \leftrightarrow T_1^{(2)}$ and $S_0^{(1)} \leftrightarrow S_0^{(2)}$ transitions (model M-1).

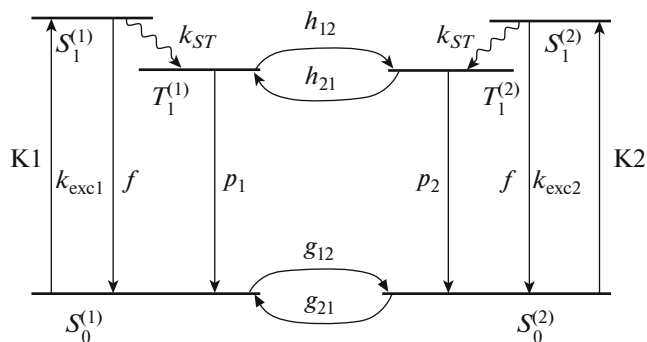


Fig. 3. Diagram of energy levels and transitions between them for the K1 and K2 metalloporphyrins complexes at the reversible K1 \leftrightarrow K2 photoconversions within the framework of the M-1 model. The straight lines and curves with arrows show rate constants: $k_{\text{exc}1}$ and $k_{\text{exc}2}$ for PhE, f for total deactivation of the S_1 state, k_{ST} for the inter-combinational conversion $S_1 \rightsquigarrow T_1$, p_1 and p_2 for the total deactivation of the T_1 state, h_{12} and h_{21} for the reversible $T_1^{(1)} \leftrightarrow T_1^{(2)}$ transitions, and g_{12} and g_{21} for the reversible dark $S_0^{(1)} \leftrightarrow S_0^{(2)}$ transitions.

It was assumed that the $S_1^{(1)}$ and $S_1^{(2)}$ levels were populated directly with PhE rates $k_{\text{exc}1}$ and $k_{\text{exc}2}$, respectively, not as a result of occupation of high levels $S_i^{(1)}$ and $S_i^{(2)}$ (not shown in the scheme) with subsequent rapid internal radiationless conversion $S_i^{(1)} \rightsquigarrow S_1^{(1)}$ and $S_i^{(2)} \rightsquigarrow S_1^{(2)}$. Such simplification reduced the number of estimated parameters without degradation of accuracy in the IPKP solution. The mathematical model in the form of the Cauchy problem without regard to the stimulated emission, intermolecular interactions, and irreversible photoprocesses had the form of an LSODE

$$\left\{ \begin{array}{l} \frac{d[S_0^{(1)}]}{dt} = -(k_{\text{exc}1} + g_{12})[S_0^{(1)}] + f[S_1^{(1)}] \\ \quad + p_1[T_1^{(1)}] + g_{21}[S_0^{(2)}], \\ \frac{d[S_1^{(1)}]}{dt} = k_{\text{exc}1}[S_0^{(1)}] - (f + k_{ST})[S_1^{(1)}], \\ \frac{d[T_1^{(1)}]}{dt} = k_{ST}[S_1^{(1)}] - (p_1 + h_{12})[T_1^{(1)}] + h_{21}[T_1^{(2)}], \\ \frac{d[S_0^{(2)}]}{dt} = -(k_{\text{exc}2} + g_{21})[S_0^{(2)}] + f[S_1^{(2)}] \\ \quad + p_2[T_1^{(2)}] + g_{12}[S_0^{(1)}], \\ \frac{d[S_1^{(2)}]}{dt} = k_{\text{exc}2}[S_0^{(2)}] - (f + k_{ST})[S_1^{(2)}], \\ \frac{d[T_1^{(2)}]}{dt} = k_{ST}[S_1^{(2)}] - (p_2 + h_{21})[T_1^{(2)}] + h_{12}[T_1^{(1)}] \end{array} \right. \quad (1)$$

with the following initial conditions and closeness:

$$[S_0^{(1)}(0)] + [S_0^{(2)}(0)] = n_1 + n_2 = [S_0^{(1)}(t)] + [S_1^{(1)}(t)] \\ + [T_1^{(1)}(t)] + [S_0^{(2)}(t)] + [S_1^{(2)}(t)] + [T_1^{(2)}(t)] = \text{const.}$$

Parameters n_1 and n_2 are the initial concentrations K1 and K2, respectively. In other models, h_{12} and h_{21} took into account essentially other transitions: $T_1^{(1)} \rightarrow S_0^{(2)}$, $T_1^{(2)} \rightarrow S_0^{(1)}$ (M-2); $S_1^{(1)} \leftrightarrow S_1^{(2)}$ (M-3); and $S_1^{(1)} \rightarrow S_0^{(2)}$, $S_1^{(2)} \rightarrow S_0^{(1)}$ (M-4).

Due to the fact that kinetic profiles were measured with a time resolution not allowing one to estimate rates of processes at stages 1, 4, and 7 the constants of which, as follows from the theoretical analysis [25], exceed the sum of the constants f and k_{ST} , the latter were specified to be similar for K1 and K2. The values $f = 2 \times 10^7$ and $k_{ST} = 3 \times 10^8 \text{ s}^{-1}$ and, correspondingly, the quantum yield of the formation of triplet states $Q = k_{ST}/(k_{ST} + f) \approx 0.9$ [21] were specified to be the same for all compounds. Such simplification, on the one hand, reduced the number of estimated parameters; on the other hand, it had a minimum effect on the results. The initial values of the rate constants p_1 and p_2 were specified and controlled such the value of $rate_{FF}$.

In the absence of PhE, populations of S_0 levels of K1 and K2 were thought to be equilibrium and determined by the equality of their interconversion rates: $g_{12}[S_0^{(1)}(t)] = g_{21}[S_0^{(2)}(t)]$ [29]. This equality made it possible to additionally reduce the number of estimated parameters by one.

The fluorescence intensity was specified as a superposition of solutions of LSODE (1): $I(t) = r_1[S_1^{(1)}(t)] + r_2[S_1^{(2)}(t)]$. Parameters r_1 and r_2 are the relative (radiating) contributions of K1 and K2, respectively, to f . Parameters n_1 , n_2 , and r_1 were estimated in the course of optimization and r_2 was set to be equal to 1 due to the sufficiency to specify only the ratio r_1/r_2 .

To establish the dependence of the process rate at stages 3 and 6 on model parameters, the analytical solution of the simplified four-level model of the LSODE close to LSODE (1) was analyzed theoretically because the latter has no explicit analytical solution. The simplification was reduced to the pairwise unification of the second–third and fifth–sixth equations of system (1), setting of the equalities $k_{exc1} = k_{exc2} = k_{exc}$ and $p_1 = p_2 = p$, as well as to the removal of f and k_{ST} . After the simplification, the system was similar to system (1) presented in [10]. As a result of reduction of the bulky solutions and neglect of knowingly small terms (when expanding some expressions in a series), it turned out that process rates within the framework of the initial model M-1 at $k_{exc1} \approx k_{exc2}$

and $p_1 \approx p_2$ were determined with a relative error of not greater than 0.1 by the expression

$$rate_{3,6}^{M-1} \approx h_{12} + h_{21} - \frac{h_{12} + h_{21} - (g_{12} + g_{21})}{1 + \Delta}. \quad (2)$$

In (2), $\Delta = k_{exc}Q/p$, and k_{exc} and p can be replaced by geometric mean values of k_{exc1} , k_{exc2} and p_1 , p_2 , respectively, in the case of pairwise closeness of their values. To preserve the approximate equality, Δ in (2) must not far exceed 1. If the triplet levels are not populated, i.e., $k_{exc}Q \ll p$, then $rate_{3,6} \approx g_{12} + g_{21}$. If $k_{exc}Q \gg p$, then $rate_{3,6} \approx h_{12} + h_{21}$. Parameter Δ is close to Δ_{FF} and, as shown in [13], Δ_{FF} is determined by the ratio of the peak intensity of stage 2 to the minimum of its intensity and shows the relative population of the T_1 level. In our investigations, Δ did not exceed 0.3.

In the case of M-3, the expression for process rates at stages 3 and 6 was obtained from the same simplified model and had a form similar to (2):

$$rate_{3,6}^{M-3} \approx h_{12} + h_{21} - \frac{h_{12} + h_{21} - (g_{12} + g_{21})}{1 + \frac{k_{exc}}{f}}. \quad (3)$$

The experimental PhE intensities were such that $k_{exc} \ll f$ always took place; as a consequence, the relatively low rate $rate_{3,6}$ in the M-3 case could be a result of the difference between the large value of the sum $h_{12} + h_{21}$ and second summand, very close to this sum. Expressions similar to (2) and (3) for M-2 and M-4 were not obtained due to the absence of the analytical solution for their simplified models. However, numerical simulation demonstrates that they are very close to (2) and (3), respectively.

Table 1 presents results of findings of rate constants of intramolecular processes, interconversions, and ratios n_1/n_2 and r_1/r_2 for the complexes of the compounds. Parameters and rate constants of photoprocesses of all four models are presented only for Zn-(*t*-Bu)₄-TBP. The relative error of the tabular data is ± 0.25 . Expressions (2) and (3) after the substitution of tabular data yield values agreeing with process rates that were obtained from experimental curves.

The quantum efficiency of conversions of K_i into K_j ($i, j = 1, 2$ and $i \neq j$) for M-1, M-2, and M-3, M-4 can be represented by the following expressions, respectively:

$$L_{ij} = Q \frac{h_{ij}}{p_i + h_{ij}}, \quad L_{ij} = \frac{h_{ij}}{f + k_{isc} + h_{ij}}.$$

It is evident that for all models $L_{ij} \approx 0.01$ (one act of conversion per 100 acts of deactivation of the S_1 or T_1 state).

Table 1. Statistically averaged values of estimated parameters and rate constants of the M-1–M-4 models*

Compound (model)	n_1/n_2	r_1/r_2	$k_{\text{exc1}}, \text{s}^{-1}$	$k_{\text{exc2}}, \text{s}^{-1}$	p_1, s^{-1}	p_2, s^{-1}	h_{12}, s^{-1}	h_{21}, s^{-1}	g_{12}, s^{-1}	g_{21}, s^{-1}
Zn-(<i>t</i> -Bu) ₄ -TBP (M-1)	1.2	0.20	900	1500	11000	4500	165	55	11	13
Zn-(<i>t</i> -Bu) ₄ -TBP (M-2)	2.0	0.24	1400	1600	13000	4000	100	65	7	13
Zn-(<i>t</i> -Bu) ₄ -TBP (M-3)	7.5	0.23	2150	900	9350	1850	5.3×10^5	1.4×10^5	7	50
Zn-(<i>t</i> -Bu) ₄ -TBP (M-4)	11	0.16	2350	750	9600	1480	3.8×10^5	2.1×10^5	5	55
Zn-TBP (M-1)	1.2	0.15	1000	1500	12000	4700	170	50	10	12
Mg-TBP (M-1)	1.4	0.4	1300	2100	10700	4700	250	30	8	5
Zn-OEP (M-1)	1.0	0.15	1050	1500	6×10^4	2×10^4	135	30	6	7

*The difference between models is noted above after the description of LSODE (1).

Discrimination of the Models

All the models exhibited almost similar matching of profiles of experimental and optimized kinetic curves at stages 3–6. This was indicated by the relative difference of compared values, which did not exceed ± 0.005 (Fig. 1, curve 3), and close OF values which differed in the magnitude not more than by 0.01. For this reason, it was impossible to take a decision in favor of one or another model by the criterion of matching of curve profiles and smallness of the OF. Calculations performed to determine the principal possibility of discrimination by OF values for M-1–M-4 with smooth (noise-free) model kinetic curves demonstrate that the kinetics can be distinguished only under the condition of total absence of noise of the analyzed curves, as well as at extremely high accuracy (at a sufficient number of significant digits) of the compared (analyzed and calculated) curves. The simulation results clearly indicate the mathematical similarity of the solutions for all the models. Noise elimination in experimental curves to extremely low (zero) values and their measurement with a very high accuracy in our experiments seemed to be almost impossible. For this reason, the discrimination was performed proceeding from the physical meaning of values of the estimated rate constants and parameters.

According to calculations, M-1 is characterized by closeness of rate constants h_{12} and h_{21} , as well as g_{12} and g_{21} , in the order of magnitude. It is evident that such situation is implemented upon the practical resonance of energies of triplet $T_1^{(1)}$ and $T_1^{(2)}$ and singlet $S_0^{(1)}$ and $S_0^{(2)}$ levels. It follows from the analysis of tabular values that the radiationless deactivation rate of K1 is higher than for K2, both in the system of singlet ($r_1 < r_2$) and in the system of triplet ($p_1 > p_2$) levels. In [30], by an example of Zn-OEP molecules, it was shown experimentally that the process of extraligation of the central metal ion led to an increase in the probability of radiationless deactivation of the T_1 state, which is caused by the participation of extraligands in the exchange of energy of electron excitation and enhancement of the

spin-orbit interaction due to macrocycle planarity distortion. Based on this, one can make an unambiguous conclusion that K1 in M-1 is a monoligated form and K2 is a nonmonoligated one. Correspondingly, the rate constants g_{12} and h_{12} characterize the process of extraligand detachment and g_{21} and h_{21} , correspondingly the process of extraligand attachment. Most probably, water, ethanol, and other mobile uncontrolled admixtures which are present in PVB and possess the coordination ability could be extraligands [31]. Extraligation is additionally corroborated by similarity of the observed nonmonotonic metalloporphyrins fluorescence kinetics to the luminescence kinetics of a europium complex [10]. In the paper, it was concluded that nonmonotonicity of the curve reflected reversible processes occurred in the rare earth complex due to the change in its ligand composition. Further, the initial equilibrium concentrations of K1 and K2 are almost equal ($n_1/n_2 \approx 1.2$). The increase in the fluorescence intensity at stage 3 is caused by the increase in concentration (in view of the fact that $h_{12} > h_{21}$) of the more luminescent K2 ($r_2 > r_1$).

As seen from Table 1, rate constants and parameters estimated by M-2 exhibited values close to M-1. This is a consequence of the fact that photoconversions K1 \leftrightarrow K2 in these models occur with the participation of lived T_1 states, and extraligation processes with similar mechanisms take place in both cases. It is seen from Table 1 that values of h_{12} and h_{21} for M-3 and M-4 are less by two or three orders of magnitude than each of the constants f and k_{ST} and exceed p_1 and p_2 by one or two orders of magnitude. Upon PhE, ligands in S_1 states detach faster ($h_{12} > h_{21}$) than attach. On the contrary, in the absence of PhE, the extraligated K1 is much more stable (n_1 exceeds n_2 by an order of magnitude).

In spite of the fact that M-3 and M-4 models exhibited high matching of profiles of experimental and optimized kinetic curves at stages 3–6, their real existence seems to be much less probable. First, exceptionally high rates of detachment–attachment of extraligands to the metalloporphyrin in the S_1 state in

a rigid polymeric matrix cannot be implemented under conditions of impeded diffuse motion of both admixtures (extraligands) and embedded porphyrins. Second, the considerable difference between h_{12} , h_{21} and g_{12} , g_{21} seems to be difficult to explain. Third, the inequality $g_{12} < g_{21}$ and, as a consequence, the prevalence of population of K1 in the S_0 state ($n_1 > n_2$) must cause, according to [30], a noticeable bathochromic shift of the long-wavelength 0–0 absorption band of this extraligated complex (for extraligated Zn-OEP, such bathochromic shift reached ~6–10 nm at 293 K and the width of 0–0 fluorescence bands was ~330–350 cm^{-1} [30]). As a result, superposition of the bathochromically shifted absorption band of K1 and band of K2 must lead to a noticeable broadening of the total long-wavelength 0–0 absorption and fluorescence band, which was not observed experimentally. The calculation demonstrated that fluorescence of the nonligated K2 complex was more effective than fluorescence of ligated K1 one, which agrees with data of [30].

The revealed rigid dependence of the process rate at stages 3 and 6 on parameters, which is expressed by (3), is also not in favor of M-3 and M-4.

CONCLUSIONS

Composite nonmonotonic fluorescence kinetic curves of some metal porphyrins in solid organic polymeric matrices have been analyzed based on the full solution of the IPKP. The rate constants and parameters of the multiparametric IPKP for the studied systems formulated in the LSODE form for four models of photoprocesses have been estimated using the Nelder–Mead derivative-free algorithm which exhibited high effectiveness and reliability. The solutions have been estimated taking into account smallness of the OF values, detailed matching of profiles of experimental and optimized kinetic curves, as well as closeness of the estimated rate constants and parameters to experimental data with preservation of the physical meaning of the hypothetical model.

The IPKP methods used make it possible to determine parameters and rate constants of processes controlling interconversions of metal complexes of tetrapyrrole macrocycles. A conclusion is made that the interconversions are caused by the reversible process of axial extraligation of the central metal ion of porphyrin, i.e., by the existence, at least, of two types of chemically nonequivalent complexes (K1 and K2). Discrimination of the models makes it possible to conclude that the reversible process of attachment–detachment of the extraligand by metal porphyrin occurs with the participation of the T_1 state (models M-1 and M-2) and, on the average, faster by an order of magnitude than in the S_0 state. Processes of axial extracoordination are considerably, at least by two orders of magnitude, slower than intramolecular pro-

cesses of PhE energy deactivation. Results of the presented investigations allow substantiatedly prove the occurrence of photoprocesses in condensed media by commonly accepted kinetic schemes.

The performed investigations are also of methodological importance. The IPKP implementation allows one to judge about the character of the interaction between admixtures or local matrix environment and embedded fluorophores and, consequently, to justify the time evolution of physico-chemical properties and quality of activated optically transparent materials.

CONFLICT OF INTEREST

The authors declare that they have no conflicts of interest.

REFERENCES

1. V. I. Dimitrov, *Simple Kinetics* (Nauka, Novosibirsk, 1982) [in Russian].
2. A. M. Denisov, *Introduction to the Theory of Inverse Problems, Tutorial* (MGU, Moscow, 1994) [in Russian].
3. S. I. Spivak, I. M. Gubaidulin, and E. V. Vaiman, *Inverse Problems of Chemical Kinetics, Tutorial* (RIOBashGU, Ufa, 2003) [in Russian].
4. S. I. Kabanikhin, *Inverse and Ill-posed Problems: Theory and Applications*, Vol. 55 of *Inverse and Ill-Posed Problems Series* (Walter de Gruyter, Berlin, Boston, 2012).
<https://doi.org/10.1515/9783110557350>
5. J. Milstein, *Modelling of Chemical Reaction Systems*, Vol. 18 of *Chemical Physics Series* (Springer, Heidelberg, 1981), p. 92.
<https://doi.org/10.1007/978-3-642-68220-9>
6. G. M. Carlson and T. Provder, *ACS Symp. Ser.* **313**, 241 (1986).
<https://doi.org/10.1021/bk-1986-0313.ch021>
7. A. L. Pomerantsev and O. E. Rodionova, *Polymer and Biopolymer Analysis and Characterization* (Nova Science, New York, 2007), Chap. 13, p. 179.
8. S. Kabanikhin, O. Krivorotko, A. Mortier, et al., *Sib. Nauch. Med. Zh.* **6** (1), 29 (2016).
9. I. V. Stanishevsky, S. M. Arabei, and T. A. Pavich, in *Proceedings of the 11th International Conference on Quantum Electronics* (RIVSh, Minsk, 2017), p. 39.
10. I. V. Stanishevsky, T. A. Pavich, and S. M. Arabei, *Opt. Spectrosc.* **126**, 111 (2019).
<https://doi.org/10.1134/S0030400X1902022X>
11. I. V. Stanishevsky and S. M. Arabei, in *Proceedings of the 12th International Conference on Quantum Electronics* (RIVSh, Minsk, 2019), p. 64.
12. I. V. Stanishevsky, in *Proceedings of the 12th International Conference on Quantum Electronics* (RIVSh, Minsk, 2019), p. 80.
13. I. V. Stanishevsky, K. N. Solov'ev, S. M. Arabei, and V. A. Chernyavskii, *J. Appl. Spectrosc.* **80**, 357 (2013).
<https://doi.org/10.1007/s10812-013-9773-9>

14. I. V. Stanishevsky, S. M. Arabei, V. A. Chernyavsky, and K. N. Solovyov, *Opt. Spectrosc.* **121**, 722 (2016).
<https://doi.org/10.1134/S0030400X16110199>
15. S. W. Provencher, *Comput. Phys. Commun.* **27**, 213 (1982).
[https://doi.org/10.1016/0010-4655\(82\)90173-4](https://doi.org/10.1016/0010-4655(82)90173-4)
16. C. Elster, J. Honerkamp, and J. Weese, *Rheol. Acta* **31**, 161 (1992).
<https://doi.org/10.1007/BF00373238>
17. A. C. Hindmarsh, *Scientific Computing* (North-Holland, Amsterdam, 1983), p. 55.
18. J. A. Nelder and R. Mead, *Comput. J.* **7**, 308 (1965).
<https://doi.org/10.1093/comjnl/7.4.308>
19. E. V. Kolesnikova, L. I. Kolesnikova, and L. Yu. Rusin, *Fiz.-Khim. Kinet. Gaz. Dinam.* **10**, 495 (2010).
20. O. I. Koifman, A. S. Semeikin, and B. D. Berezin, *Porphyrins: Structure, Properties, Synthesis* (Nauka, Moscow, 1985) [in Russian].
21. V. A. Kuz'mitskii, K. N. Solov'ev, and M. P. Tsvirko, *Porphyrins: Spectroscopy, Electrochemistry, Application* (Nauka, Moscow, 1987) [in Russian].
22. T. A. Pavich, S. M. Arabei, and K. N. Solovyov, *J. Appl. Spectrosc.* **85**, 1 (2018).
<https://doi.org/10.1007/s10812-018-0603-y>
23. Scilab. <https://en.wikipedia.org/wiki/Scilab>.
24. F. Gao and L. Han, *Comput. Optim. Appl.* **51**, 259 (2012).
<https://doi.org/10.1007/s10589-010-9329-3>
25. I. Fajfar, A. Bürmen, and J. Puhan, *Optimiz. Lett.* **13**, 1011 (2019).
<https://doi.org/10.1007/s11590-018-1306-2>
26. Maxima.
[https://en.m.wikipedia.org/wiki/Maxima_\(software\)](https://en.m.wikipedia.org/wiki/Maxima_(software)).
27. S. M. Arabei, J.-P. Galaup, K. N. Solovyov, and V. F. Donyagina, *Chem. Phys.* **311**, 307 (2005).
<https://doi.org/10.1016/j.chemphys.2004.10.045>
28. I. V. Stanishevsky, in *Proceedings of the 11th International Conference on Quantum Electronics* (RIVSh, Minsk, 2017), p. 369.
29. I. V. Stanishevsky and K. N. Solovyov, *Opt. Spectrosc.* **96**, 221 (2004).
<https://doi.org/10.1134/1.1651247>
30. V. N. Knyukshto, A. M. Shul'ga, E. I. Sagun, and E. I. Zen'kevich, *J. Appl. Spectrosc.* **65**, 943 (1998).
<https://doi.org/10.1007/BF02675753>
31. N. Zh. Mamardashvili, V. V. Borovkov, G. M. Mamardashvili, Y. Inoue, and O. I. Koifman, *Chemical Processes with Participation of Biological and Related Compounds. Biophysical and Chemical Aspects of Porphyrins, Pigments, Drugs, Biodegradable Polymers, and Nanofibers* (Koninklijke Brill, Leiden, 2008), p. 117.